PFG – Journal of Photogrammetry, Remote Sensing and Geoinformation Science
https://doi.org/10.1007/s41064-024-00277-z

ORIGINAL ARTICLE

Disaster Risk Assessment of Fluvial and Pluvial Flood Using the Google Earth Engine Platform: a Case Study for the Filyos River Basin

Hakan Akcin[1] · **Ruveyda Tercan Kose**[2]

Received: 30 September 2023 / Accepted: 30 January 2024

Abstract
The aim of this study is to conduct a risk analysis of fluvial and pluvial flood disasters, focusing on the vulnerability of those residing in the river basin in coastal regions. However, there are numerous factors and indicators that need to be considered for this type of analysis. Swift and precise acquisition and evaluation of such data is an arduous task, necessitating significant public investment. Remote sensing offers unique data and information flow solutions in areas where access to information is restricted. The Google Earth Engine (GEE), a remote sensing platform, offers strong support to users and researchers in this context. A data-based and informative case study has been conducted to evaluate the disaster risk analysis capacity of the platform. Data on three factors and 17 indicators for assessing disaster risk were determined using coding techniques and web geographic information system (web GIS) applications. The study focused on the Filyos River basin in Turkey. Various satellite images and datasets were utilized to identify indicators, while land use was determined using classification studies employing machine learning algorithms on the GEE platform. Using various applications, we obtained information on ecological vulnerability, fluvial and pluvial flooding analyses, and the value of indicators related to construction and population density. Within the scope of the analysis, it has been determined that the disaster risk index (DRI) value for the basin is 4. This DRI value indicates that an unacceptable risk level exists for the 807,889 individuals residing in the basin.

Keywords Fluvial and pluvial flood · Forest fire · Disaster risk index · GEE · Machine learning

1 Introduction

Disasters occur due to natural, human-induced, or technological hazards that may cause damage to society and the environment at any time. Major natural disasters are floods, earthquakes, landslides, hurricanes, volcanic eruptions, forest fires, storms, and droughts (IFRAC 2023; SAMHSA 2023). Some of the human-caused or technological ones are nuclear and chemical accidents, major fires, illegal construction, dam collapses, terrorist incidents, wars, and lack of energy and materials (Dalezios et al. 2017; Teh and Khan 2021). Since loss of life and property often occur in societies as a result of an undesirable hazard or event, it is necessary to make assessments regarding the extent of risk posed by these threats and to take precautions to reduce the disaster risk (IRDR 2014). The United Nations Environment Program reports that more than 2 billion people have been affected by disasters and conflicts since the year 2000 and have witnessed more than 2500 disasters since the beginning of this century (UNEP 2023). The report states that these tragic events have destroyed infrastructures, displaced populations, and fundamentally undermined human security. They are also reported to increase poverty and tear apart the fabric of sustainable development. Therefore, in societies prone to disasters, determining the potential for possible losses due to the vulnerability of the social situation and ecological system is an important issue (Peng 2018; Takamatsu and Abhas 2023).

Risk refers to the chance of a particular adverse event happening within a certain timeframe; thus, it is important to define the potential for harm resulting from hazard. Risk assessment involves appraising and categorizing the risks that arise from hazards, alongside the factors that

✉ Hakan Akcin
akcinh@beun.edu.tr

[1] Department of Geomatics Engineering, Zonguldak Bulent Ecevit University, Zonguldak, Turkey

[2] Department of Geomatics Engineering, Graduate School of Natural and Applied Sciences, Zonguldak Bulent Ecevit University, Zonguldak, Turkey

Published online: 08 March 2024

can convert hazards into risks, in order to ascertain control measures (Deck et al. 2009; Akcin 2021). Risk control can be achieved by systematically assessing appropriate measures for each risk group. This process evaluates hazard identification data and guides strategic decisions. Accurate risk assessment, particularly of fluvial (river floods) and pluvial flood (flash floods) in coastal regions, is essential. However, the majority of disaster analyses primarily focus on economic losses by neglecting indicators associated with exposure to hazards and characteristics of the disaster (Peng 2018). Accessing information and data regarding these indicators is challenging and requires considerable effort at high costs. Remote sensing-based solutions are the only viable alternative that can provide a steady data and information flow in geographies where access to such information is limited and laboriously obtained (Anaya et al. 2020; Takamatsu and Abhas 2023).

The main academic contribution of this research is to conduct a disaster risk appraisal of the susceptibility of inhabitants residing in the watershed of coastal areas to fluvial and pluvial flood hazards. This appraisal is solely based on datasets and remote sensing images acquired through the Google Earth Engine (GEE) platform. The case analysis for disaster risk assessment was carried out for the Filyos basin in the western Black Sea coastal region of Turkey, shown in Fig. 1. Coastal regions in Turkey exhibit various climatic conditions. The country's shores experience Mediterranean, Black Sea, and transitional Marmara climates. On the coasts where the Black Sea climate prevails, a substantial amount of precipitation may occur, which requires protective measures against risks, including flooding (Buyuksalih et al. 2005, Seker et al. 2005; Akyüz et al. 2014; Şarlak 2014; Sönmez and Kale 2020). In certain areas of the western

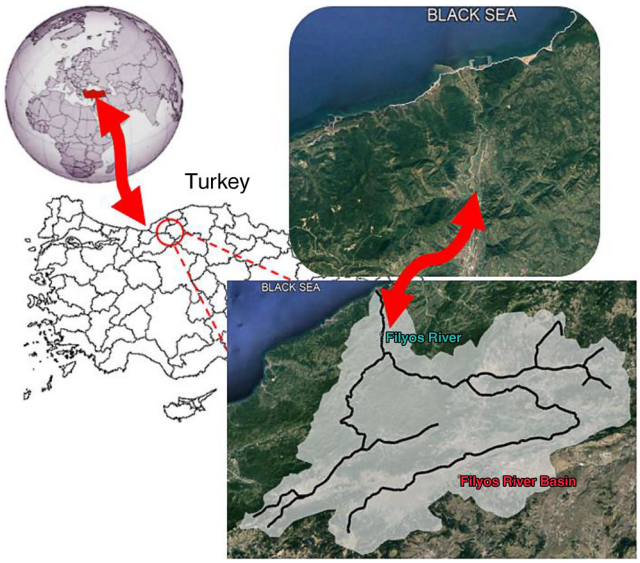

Fig. 1 Location of case study area: Filyos River basin

Black Sea ecosystem, several factors including forest fires, deforestation, agriculture, industry, housing, tourism, and transport development push the environment to rapidly deteriorate (TOD 2022). Turkey's Filyos River and its basin is one such location. In this context, a legal regulation has been passed by the Ministry of Agriculture and Forestry of the Republic of Turkey, General Directorate of Water Management, based on the European Union Flood Directive (Directive 2007/60/EC of the European Parliament and of the Council on the Assessment and Management of Flood Risks 2007). This regulation dated 12 May 2016 on the preparation, implementation, and monitoring of flood management plans of the western Black Sea basin, which includes the Filyos River basin, covers the measures to be taken, activities to be carried out, and distribution of responsibilities for the management of flood risks in the basin. This directive and legal regulation is the main reason why the Filyos basin was selected and examined in this study.

The Filyos River has a length of 312 km. Its catchment area is 13,300 km^2 and covers five provinces. The annual mean precipitation is 1200 mm in the basin's coastal regions and 600 mm at its internal areas (Küçükali 2019).

The area north of the basin, which is governed by the legal regulations of the Filyos Valley Project, is currently undergoing rapid development and turning into a vast industrial district which is at the risk of ecological degradation as well as fluvial and pluvial floods. Within the scope of fluvial and pluvial flood disaster risk assessment of this basin belongs to the GEE platform, Climate Hazards InfraRed Precipitation with Station data (CHIRPS), climate reanalysis of Copernicus Climate Change Service European Reanalysis (ERA), World Wildlife Fund (WWF) HydroSHEDS Hydrographic Data, Space Filled Digital Elevation Model (DEM) and Joint Research Centre (JRC) Surface Water Mapping, NASA Socioeconomic Data and Applications Center (NASA SEDAC) at the International Earth Sciences Information Network Center, Fire Information for Resource Management System (FIRMS) and Landsat - Hansen Global Forest Change v1.9 medium resolution datasets, Landsat-8, MODIS and Sentinel-1 SAR medium resolution satellite images considered as quantitative indices for disaster risk assessment. First, datasets and images were used to identify indicators of hazard exposure. Then, vulnerability indicators were identified, followed by disaster prevention indicators.

2 Methodology and Data for Risk Assessment

The disaster risk index (DRI) method was chosen for the factors and indicators determined by taking into account the principles of fluvial and pluvial flood disaster risk formation

and the physical and social characteristics of the study area. In order to perform an evaluation with this method, a web geographic information system (GIS) application was used by writing code on the GEE platform, and the indicator values to be used in DRI evaluation were determined.

2.1 DRI Method

DRI is a crucial indicator that shows the extent of risk exposure on various scales for different hazards that regions may face, whether large or small, as well as the level of risk identification and management (Ramli et al. 2019). To determine disaster risk arising from fluvial and pluvial floods, the DRI model employs three selected factors. The first one is the hazard factor. There are different indicators regarding the hazard factor that occur within the concept of space and time. It is necessary to determine the scale and impact of these indicators. The evaluation approaches vary across countries and regions. The second factor chosen in the DRI model is vulnerability (Chang and Chao 2012). This is a factor that explains why different people who are subjected to the same event may have high or low risk depending on the physical and social situation. Another factor is the ability to prevent and mitigate disaster risk, with indicators that have varying impacts depending on the structure of societies that are exposed to disasters and the approaches adopted by countries to address this problem (Peduzzi 2006; Karmakar et al. 2010; Islam et al. 2013; Bathrellos et al. 2016; Hernández et al. 2018). The potential risk value can be determined using the Eq. 1 provided below (Hu et al. 2009; Ramli et al. 2019).

$$DRI = f(H, V, R) = F_H * W_H + F_V * W_V + F_R * W_R \quad (1)$$

In this function, "H" the hazard, "V" the vulnerability, and "R" the capability of disaster prevention and reduction; F_H is the factor of hazard, F_V the factor of vulnerability, F_R the factor of reduction; W_H, W_V, and W_R are the factor weights.

2.2 Data Requirement for Fluvial and Pluvial Flood Hazard Analysis

Fluvial and pluvial flood hazards, which are among the most common disaster types in the world, are also among the most damaging natural disaster types. The indicators determined for the hazard factor, vulnerability factor, and disaster prevention factor will be used in fluvial and pluvial flood risk estimation. These indicators, which are so important and have disaster-sized results, are as follows:

- *Land use/land cover*: Plants protect the soil, cover, and regulate flow (Stefanidis and Stathis 2013). Destruction of land covered by construction increases the flow volume (Kandilioti and Makropoulos 2012).
- *Precipitation*: Excessive rainfall occurring in a short period of time is the most important indicator that causes floods (Wang et al. 2015). For risk assessment, it is necessary to determine standardized precipitation indices and determine the number of precipitation repetitions through time series analysis.
- Size and number of areas affected by floods in the past.
- The size of the decrease in forested areas.
- *River flood index (RFI):* RFI is an important indicator in terms of hydrological applications, transportation, and disaster risk management. This index was developed by the Copernicus Climate Change Service as a 30-year average river flood index (50-year flood recurrence level) distribution using the E-HYPERGRID hydrological model and a combination of eight climate models for historical and future periods (Product user guide European river flood explorer 2022).
- *Relative sea level rise (RSLR) in river delta*: If the area where the flood occurred includes coastal areas and river deltas, it is important to obtain the size of the sea level rise. This dataset is based on reanalysis data available in the Copernicus Climate Change Service (C3S) climate data repository. Long-term time series of compiled observational and simulated index data were used for this analysis (Product user guide European relative sea level rise explorer 2022).
- Population at risk.
- *Building density in the delta and on riverbanks*: Building density and quality (building types, building materials, number of floors, maintenance level) are responsible for the distribution of physical vulnerability (Thouret et al. 2024). Objects and structures that can be carried away by floods are considered as vulnerable.
- *Ecological vulnerability elements*: Environmental elements (ecosystems, protected areas, environmentally sensitive areas, forests, wetlands, flora, fauna, biodiversity, aquifers) can also be damaged by flood disaster (Van Westen et al. 2008).

Weights for each factor and indicator covering the data provided for fluvial and pluvial flood hazard assessment by the DRI method are handled with two approaches. The first of these is to determine the weights based on expert opinion for factors and indicators specific to the region to be evaluated, and the second is to determine the weights based on analytic hierarchy process (AHP) analyses with GIS (Schumann et al. 2011; Peng 2018).

While some countries such as Indonesia and Brazil chose equal weights in the selection of these weights, countries such as China, Pakistan, and Vietnam used different weighted values. In the USA, both are included in

Table 1 Weighted values of the factors and indicators of the disaster risk index (DRI)

Disaster risk index			
Factor level		Indicator level	
Factor	Weighted value	Indicator	Weighted value
F	W_F	I	W_I
Hazard	0.45	Number of flood recurrences (year)	0.20
		Size of the flood affected area (ha)	0.20
		SPI	0.20
		Loss of forest areas (ha)	0.10
		RFI (m^3/s)	0.15
		RSLR in river delta (cm)	0.15
		–	[ ] = 1.0
Vulnerability	0.40	Population (person)	0.16
		SVI	0.10
		EVI	0.10
		LST (°C)	0.10
		Temperature (°C)	0.10
		AOD	0.10
		AET	0.10
		Number of forest fires	0.12
		Building density in delta and riverside (%)	0.12
		–	[ ] = 1.0
Capability of preventing and reducing disaster	0.15	Observation frequency (months)	0.50
		Urbanization level (%)	0.50
	[ ] = 1.0	–	[ ] = 1.0

SPI standardized precipitation index, *RFI* river flood index, *RSLR* relative sea level rise, *SVI* standardized vegetation index, *EVI* enhanced vegetation index, *LST* land surface temperature, *AOD* aerosol optical depth, *AET* actual evapotranspiration

Table 2 Evaluation of the risk result defined according to the factors and indicators

Value of DRI	Assessment	Activity
4 and 5	Unacceptable risk	*The municipalities and relevant ministry must immediately take action in relation to this risk*
2 and 3	Remarkable risk	*The municipalities and relevant ministry should interfere as soon as possible*
1	Acceptable risk	*It can be intervened in the longer term by keeping it under surveillance*

the analysis (Ramli et al. 2019). In this study, weights were determined with expert opinions, and different weighted values are presented in Table 1. The categorical evaluation to determine the level of DRI results is shown in Table 2. According to the results of this evaluation, relevant local governments, public institutions, and ministries will quickly complete their preparations by issuing an action plan to reduce the risk.

2.3 GEE Algorithm with Images and Datasets

In the study aiming to determine indicator values for spatial and temporal disaster risk assessment for the Filyos River basin between 2000 and 2022 using the GEE platform, classification studies were firstly carried out to determine land cover and use with Landsat 8 images. In the classification, thematic classes were determined with random forest (RF) unsupervised classification, which is a machine learning (ML) algorithm. Using MODIS satellite data, SVI and EVI vegetation indices, AET plant moisture content, LST land surface temperature, and AOD air pollution parameters for the basin were calculated for the time period of 2000–2022, and time series analysis of these indices and parameters was performed. Indicators for disaster assessment were obtained using some datasets. Out of these, the SPI precipitation index was determined by the CHIRPS Daily Climate Hazard Identification Group using satellite infrared measurements and station data, and a time series analysis was also performed. The population density of the basin was determined and mapped with NASA SEDAC at the International Earth Sciences Information Network Center datasets.

The FIRMS (Fire Information for Resource Management System) dataset was used to determine the number of detections of forest fires that occurred in the basin. The

Table 3 Data used in the study

Data	Dataset time range	Dataset provider	Data Resolution
SPI	1981-01-01–2022-10-31	CHIRPS Daily: Climate Hazards Group InfraRed Precipitation with Station Data (Version 2.0 Final)	0.05°
	2000-02-18–2022-09-30	MODIS MOD13Q1.006 Terra vegetation indices (16-day global)	250 m
EVI	2000-02-18–2022-09-30	MODIS MOD13Q1.006 Terra vegetation indices (16-day global)	250 m
Temperature, RFL index, RSLR	1979-01-01–2020-06-01	Copernicus Climate Change Service—European Reanalysis 5 (ERA5) monthly temperature data	0.25°
Land surface temperature, LST	2000-02-18–2022-11-01	MODIS MOD11A2.061 land surface temperature data (8-day global)	1000 m
AOD	2000-02-01–2022-10-01	MODIS MOD08 _ M3. 061 Terra atmosphere aerosol data (monthly global)	1° × 1°
Evapotranspiration	2001-01-01–2022-10-24	MODIS MOD16A2. 006 Terra net evapotranspiration data (8-days global)	500 m
Fluvial and pluvial flood	2014-10-03–2022-11-19	Sentinel-1 SAR GRD: C-band synthetic aperture radar ground range data	10 m
	2000-02-11–2000-02-22	WWF HydroSHEDS: hydrographic data, space-filled DEM.	3 arc seconds
	1984-03-16–2022-01-01	JRC surface water mapping	30 m
Population	2000-01-01–2020-01-01	NASA SEDAC at the International Earth Sciences Information Network Center, GPWv411: UN adjusted population density data	30 arc second
Number of fires	2000-11-01–2022-11-08	FIRMS (Fire Information for Resource Management System) data	1000 m
Forest losses	2000-01-01 2021-01-01	Landsat—Hansen Global Forest Change v1.9 data	1 arc second
Building footprint	2014–2021	Buildings (Maxar, Airbu, and IGN France images)	15.4 m/pixel

Landsat—Hansen Global Forest Change v1.9 dataset was evaluated to determine the losses of forest assets in the basin. The Building Footprints (Buildings; Maxar, Airbus, and IGN France Images) dataset was used to determine the urbanization level and building density. The data of the study, the sources of the data, the time intervals, and the resolution values are summarized in Table 3.

3 Results Obtained with the GEE Application

3.1 SPI Values of the Basin

SPI values range from -2 to +2. When conducted a drought assessment using SPI values, a time period falling below zero indicates drought, while values above zero suggest thatdrought has decreased, meaning precipitation has increased (McKee et al. 1993). Furthermore, if a value above 0.5 is observed during a dry season, it implies that there is a possibility of floods caused by sudden rainfall. Between 2000 and 2022, the SPI was 0.1. The highest SPI reading of 1.84 was recorded in June 2021 during the summer period, while the lowest SPI of –1.16 was registered in December 2015 in the winter season. Figure 2 illustrates the SPI time series graph, indicating that flood disasters tend to arise in biennial intervals when SPI values surpass 1.50. Additionally, Fig. 3 depicts the SPI map of the basin dated 30 September 2022.

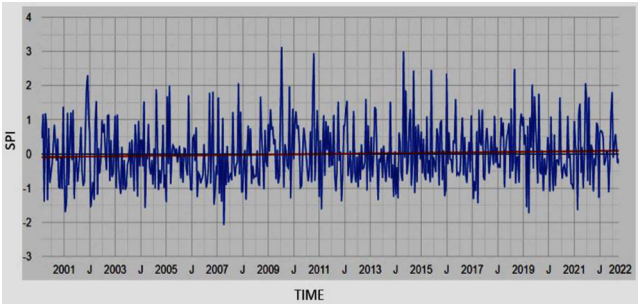

Fig. 2 Standardized precipitation index (*SPI*) time series graph between 2000 and 2022

3.2 SVI and EVI Values of the Basin

To access mean variations in vegetation and drought during a specific time period, SVI index values were obtained from 2000 to 2022, employing the Terra vegetation indices of the MODIS satellite. As per the data, the maximum SVI value

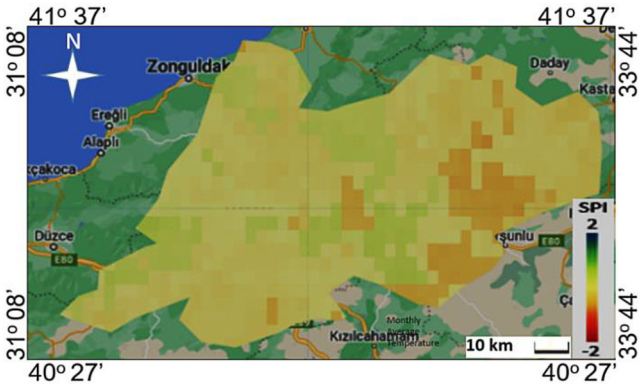

Fig. 3 Standardized precipitation index map dated 30.09.2022

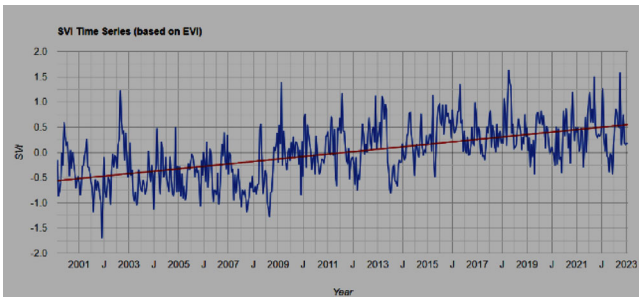

Fig. 4 Standardized vegetation index (*SVI*) time series graph between 2000 and 2023

recorded between 2000 and 2022 was in 2018 with 1.51, while the minimum SVI value was identified in 2008 with –1.21. Upon examination of a 22-year general average, it was discovered that the value was 0.00 and subsequently determined to have no impact on drought occurrence in the region. The Filyos River basin SVI time series graph is displayed in Fig. 4, while Fig. 5 illustrates the SVI map between January 17, 2023, and February 2, 2023.

To assess plant growth in the basin, we obtained EVI values from the Terra vegetation indices of the MODIS satellite

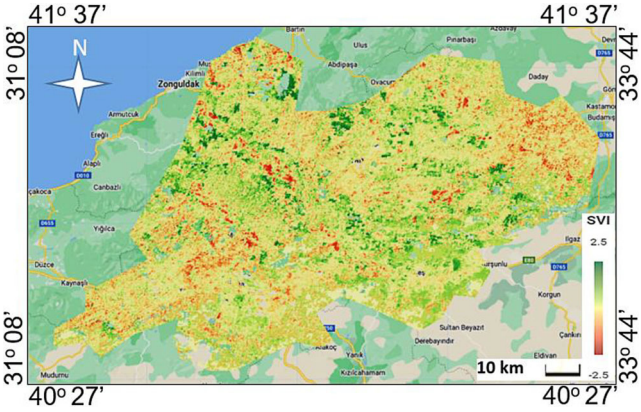

Fig. 5 Standardized vegetation index map between 17.01.2023 and 02.02.2023

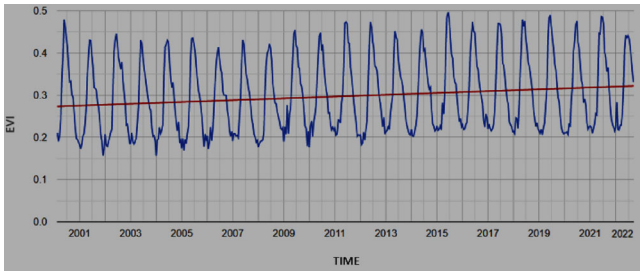

Fig. 6 Enhanced vegetation index (*EVI*) time series graph between 2000 and 2022

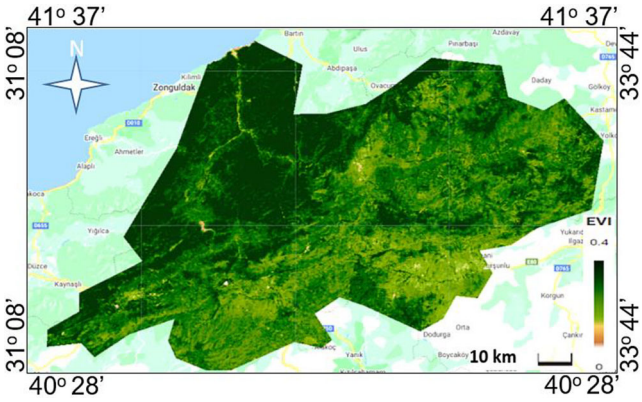

Fig. 7 Enhanced vegetation index map between 14.09.2022 and 30.09.2022

between 2000 and 2022. These values enable evaluation of biomass and drought conditions in the area. The peak EVI value, which can fluctuate within the range of –1 to 1 in the basin from 2000 to 2022, was ascertained to be 0.49 in both 2015 and 2021. The lowest was recorded in 2001 at 0.17. When considering the general average of 22 years, a value of 0.30 is observed. This value corresponds to the average density of the plant density class that has developed in the region. Figure 6 presents the EVI time series graph, while Fig. 7 depicts the EVI map between 14.09.2022 and 30.09.2022.

3.3 Temperature Values of the Basin

In the GEE application, temperature values, which were among the factors causing climate change between 2000 and 2020, were obtained with ERA5 temperature data within the Copernicus program. The average temperature between 2000 and 2020 was 10.75 °C. The lowest average temperature was observed in 2011 with 9.95 °C, and the highest average temperature was observed in 2010 with 12.27 °C.

During the study years, the highest temperature was seen in August 2010 with 23.78 °C, and the lowest temperature was in January 2000 with –2.87 °C. The monthly average temperature time series graph between 2000 and 2020 is

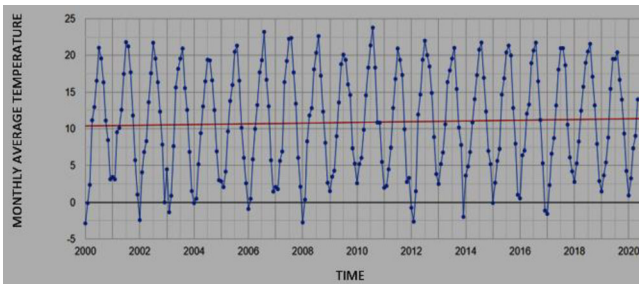

Fig. 8 Monthly average temperature time series graph between 2000 and 2020

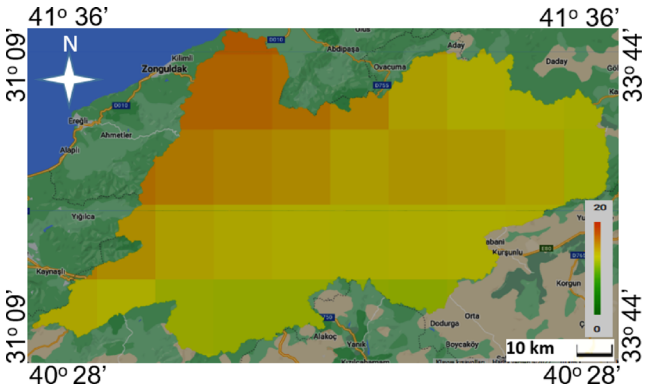

Fig. 9 Monthly average temperature map between 2000 and 2020

given in Fig. 8. The average temperature map between 2000 and 2020 is shown in Fig. 9.

3.4 LST Values of the Basin

The present study acquired LST data of the Filyos River basin spanning 2000 to 2022 through utilization of the MOD11A1.061 module of the MODIS satellite. The average annual LST value for this time period was 16.81 °C, with the maximum annual average of 20.31 °C occurring in 2000 and the minimum annual average of 15.38 °C in 2011. Based on the study months, the LST value reached its peak in July 2007 at 34.18 °C, and hit its lowest point in January 2012 at –4.40 °C. Figure 10 displays the monthly average LST time series chart from 2000 to 2022 according to the

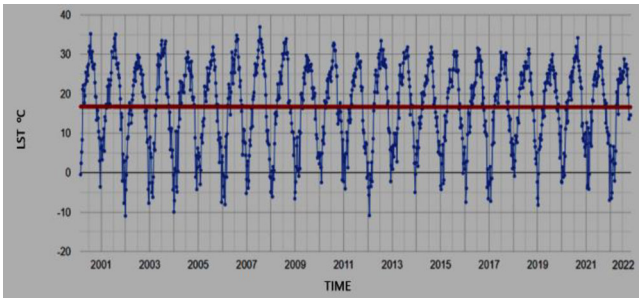

Fig. 10 Land surface temperature (*LST*) time series chart between 2000 and 2022

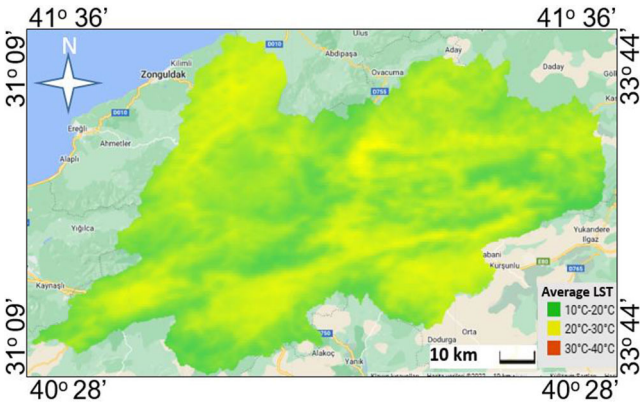

Fig. 11 Land surface temperature map of basin between 2000 and 2022

data collected. Additionally, Fig. 11 illustrates the average LST map of the basin from 2000 to 2022.

3.5 AOD Values of the Basin

The average AOD between 2000 and 2022 was 0.18 as determined through an examination of satellite and atmospheric data on harmful substance concentrations in the air using the MODIS MOD08_M3.061 Terra module. The highest annual AOD average was calculated in 2002 and 2011 (0.21), while the lowest was recorded in 2021 (0.16) during the study period. On a monthly basis during the study period, the highest AOD reading of 0.32 was recorded in April 2008, while the lowest reading of 0.09 was observed in January 2001 within the basin. The study has revealed that the mean values are similar to those found in Turkey. The time series graph depicting the average AOD is illustrated in Fig. 12, whereas the average AOD map ranging from 2000 to 2022 is presented in Fig. 13.

3.6 AET Values of the Basin

The investigation focused on the impact of AET values on the climate, considering their representation of actual transpiration and evaporation from water surfaces and plants.

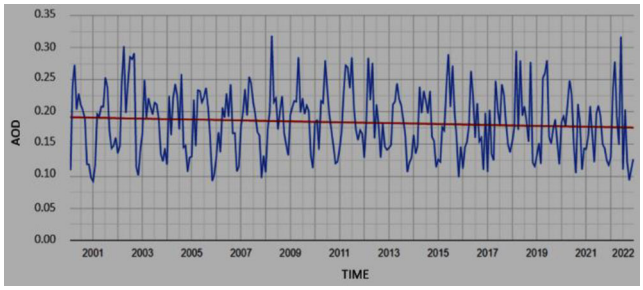

Fig. 12 Average aerosol optical depth (*AOD*) time series graph

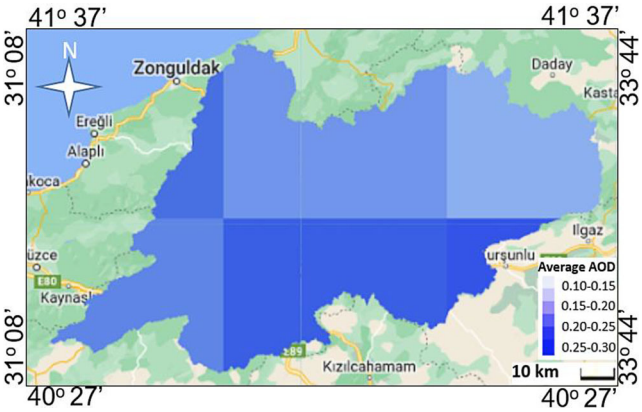

Fig. 13 Aerosol optical depth map of the basin between 2000 and 2022

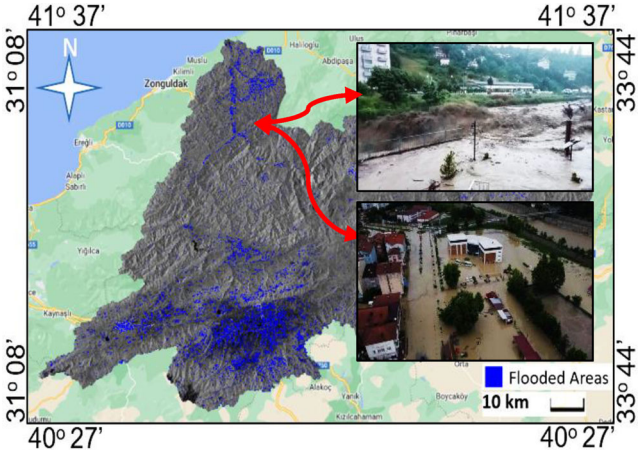

Fig. 15 Areas of the region were flooded following the flood that occurred on August 11, 2021

The obtained AET values between 2001 and 2021 indicate an increase during summer and decrease in winter.

The study data reveal that the region experienced the highest total AET value for evaporation and transpiration in 2021, with 16.75 kg/m²/8 days. Conversely, the lowest total AET value occurred in 2007 with 14.03 kg/m²/8 days. The AET average between 2000 and 2021 was 15.47 kg/m²/8 days. On a monthly basis, evaporation and transpiration peaked in June 2017 at 3.09 kg/m²/8 days, while their minimum occurred in December 2001 at 0.30 kg/m²/8 days. The temporal change of AET is presented in Fig. 14.

3.7 Fluvial and Pluvial Flood Values of the Basin

The aim of this implementation was to produce a flood map that displays the affected areas due to the floods. Flooded regions were identified by comparing Sentinel-1 SAR GRD C-band synthetic aperture radar ground range satellite data before and after the flood event in conjunction with WWF HydroSHEDS hydrographic data. The study analyzed the impacts of flooding and overflow events in the Filyos River basin. Figure 15 presents the extent of flooding and the flood event on 11 August 2021 in the affected areas. The analysis indicated that the excessive rainfall, flooding, overflows, and landslides in the basin had the most significant impact in the southwestern part of the Filyos basin. Moreover, the affected areas were extensive, amounting to 57,559 ha in the region. Figure 16 illustrates the extent of the impact of excessive rainfall, floods, and flash floods experienced

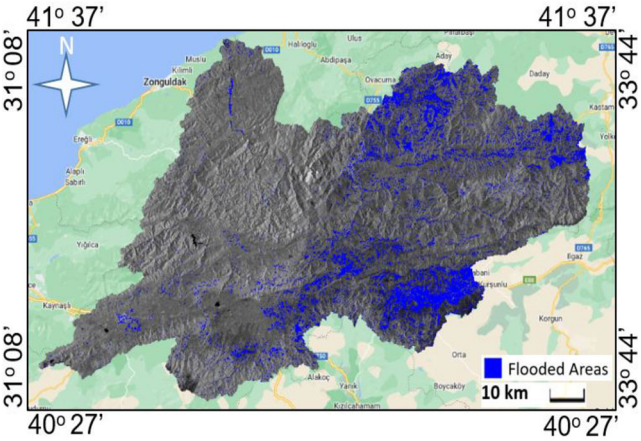

Fig. 16 The flooding event that occurred on June 27, 2022, resulted in the flooding of various areas

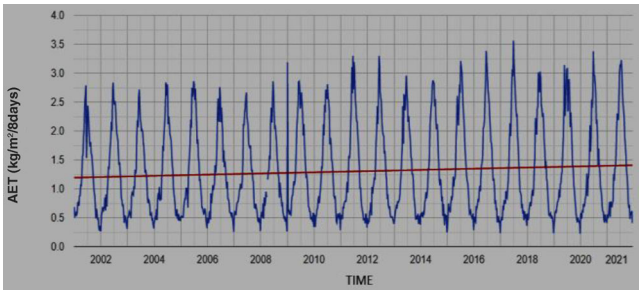

Fig. 14 Temporal change of actual evapotranspiration (*AET*) in basin

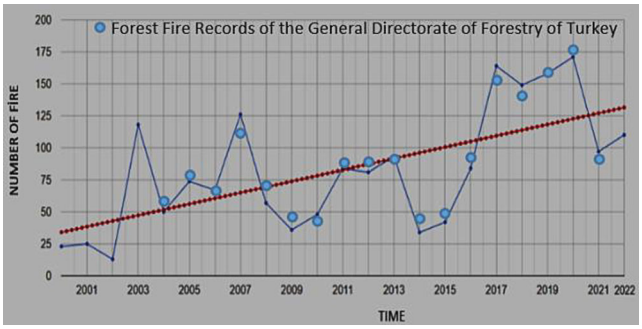

Fig. 17 The time series graph of the number of fires in the Filyos basin between 2000 and 2022

Fig. 18 Map of the fire occurrence points within the basin

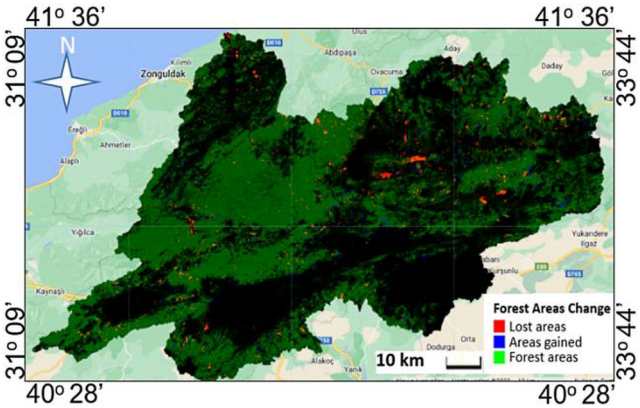

Fig. 20 Forest lost areas in the basin between 2000 and 2021

in the same region on June 27, 2022, which was found to cover an area of 98,418 ha.

3.8 Number of Fires, RFL Index, and RSLR Values in the Basin

Fires in the Filyos River Basin was analysed using data of FIRMS from the GEE platform. The basin experienced the highest number of fires in 2020 with 171, and the lowest number in 2002 with only 13. A time series graph showcasing the fire occurrences between 2000 and 2022 is presented together with the forest fire records from the General Directorate of Forestry of Turkey in Fig. 17, and the locations of the fire incidents within the basin are displayed on the map presented in Fig. 18. The RFL value within the basin was determined to be 372, while the RSLR value was measured at 7.6 cm according to the Copernicus Climate Change Service.

3.9 Forest Lost Areas and Building Footprints in the Basin

The global forest extent and change were analyzed via the Hansen Global Forest Change study. Utilizing Landsat satellite imagery, a time series analysis was undertaken to scrutinize forest area alterations. Figure 19 illustrates the time series graph depicting changes in forest area in the Filyos basin from 2001 to 2021. Figure 20 represents a corresponding map. Based on the study findings, the greatest annual loss of forest area between 2001 and 2021 occurred in 2021, with a total of 1908 ha. In contrast, the smallest annual loss of forest area was observed in 2001, with a mere 39 ha. The relationship of the building footprint density distribution shown in orange color on the satellite image with the basin boundaries and the Filyos River is presented in Fig. 21.

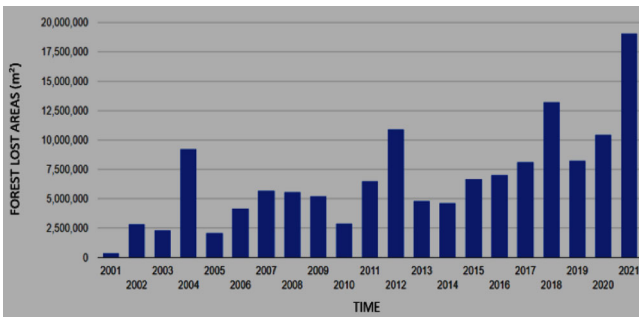

Fig. 19 The forest area change time series graph of the Filyos basin between 2001 and 2021

3.10 Population in the Basin

Population data for the Filyos Basin between 2000 and 2020 were analyzed using the GPWv411 product provided by NASA.

Figure 22 illustrates the map showcasing the relationship between population density and the Filyos River in the basin for 2020. The population within the basin increased from 699,587 in 2000 to 807,889 in 2020.

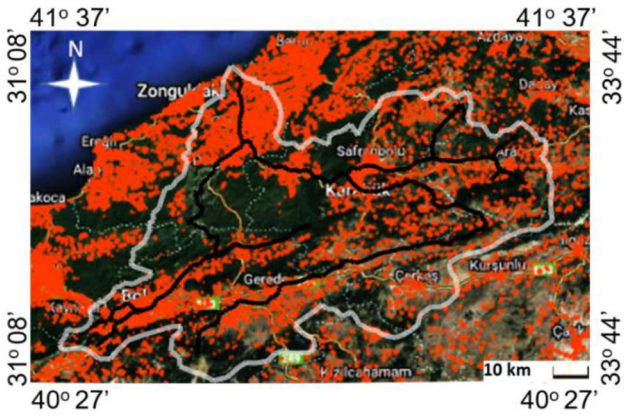

Fig. 21 Building footprints (in *orange*) map

3.11 Land Cover and Use in the Basin

For assessment of fluvial and pluvial flood risk indicators in the Filyos River basin, the most suitable Landsat 8 satellite images, captured by GEE and with a cloud coverage of less than 10%, were chosen. These images were then classified to determine the land cover and use of the Filyos River Delta and its environs. Random Forest (RF) was selected as the machine learning algorithm for classification due to its proven success as stated in Rodriguez-Galiano (2012), Du et al. (2021) and Abubakar et al. (2023). The application identified forested areas, wetlands, artificial features (highways, airport, seaports, railway, structures, etc.), dunes, cultivated and uncultivated land, dry areas, and coastal structures. The resulting classification map is presented in Fig. 23, and Table 4 provides the accuracy percentage values of the algorithm.

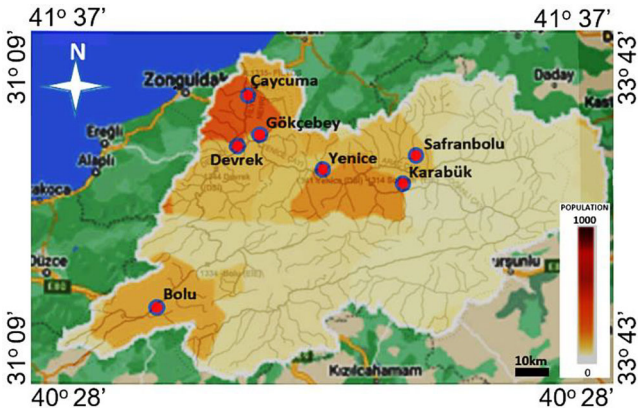

Fig. 22 Relationship map between the population density and the Filyos River in the basin

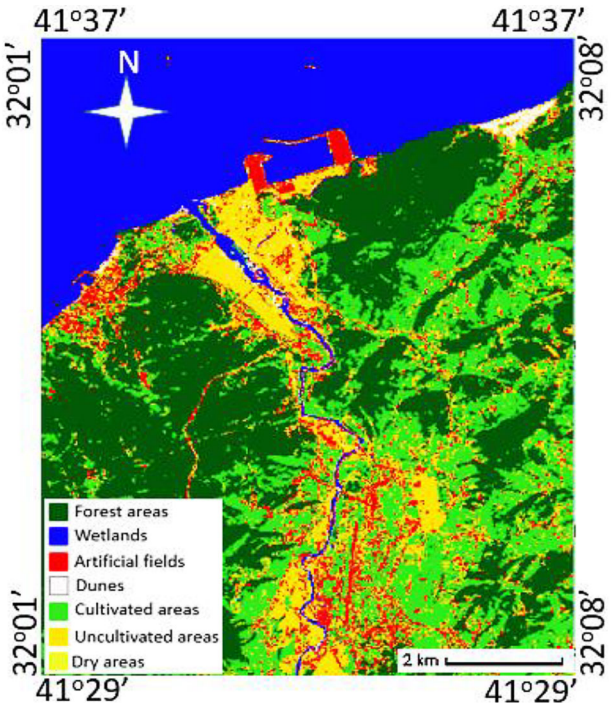

Fig. 23 Classified map of the Filyos River Delta and its environs dated 30.08.2022

3.12 Results for DRI Assessment

The assessment results for the DRI method, obtained using indicators of the Filyos River basin, are presented in Table 5. According to this evaluation, the risk value for the Filyos River basin was determined to be 4. This value exceeds the remarkable and acceptable risk levels according to the assessments outlined in Table 2.

4 Discussion

Spectral indices can be utilized to determine the drought conditions of the basin effectively through the GEE platform. Additionally, burning rates of plants, water rates in plants, and water areas can also be assessed. Evaluations in terms of live and healthy vegetation can be carried out using this platform. The higher-than-normal annual average values of drought-indicating SVI and EVI indices in the Filyos River basin are perceived as a positive factor in reducing disaster risks. Nonetheless, elevated SPI and RFI values, chiefly during the dry season, imply that the basin experiences river floods and pluvial floods during these periods. High AOD and AET values are believed to increase the likelihood of disaster, while LST and atmospheric temperature levels have been found to be within normal ranges. Nevertheless, LST and atmospheric temperature levels are expected to impact evaporation in the basin, leading to an increase in precipitation.

It has been established that forest fires and losses in the basin are more frequent than usual. It is a known fact that plants and forests safeguard the soil cover and regulate flood flow. Moreover, it is believed that the destruction of tissue particularly amplifies the volume of the flow. Therefore, the high levels of losses are deemed to enhance the risk of disaster. Another finding in the basin is that there are higher construction rates on both banks of the river and in the delta. Buildings have various characteristics that make the people living in them vulnerable to hazards. It is recognized that these building features contribute to the unequal distribution of vulnerability.

After the evaluation, it was concluded that areas with high population density in the basin are at a heightened risk of vulnerability. This is due to the potential destruction hazard of buildings caused by floods.

Seventeen different indicators examined on the GEE platform were used for the factors discussed in this study. Some of the indicators, each with independent features,

Table 4 Landsat 8 RF classifier accuracy assessment results of the delta and its environs for 2022

Classes evaluated with RF classifier	User accuracy	Producer accuracy	Overall accuracy	Kappa coefficient
Forest areas	0.99	0.98	0.85	0.78
Wetlands	0.97	0.96		
Artificial areas	0.73	0.74		
Dunes	0.75	0.65		
Cultivated areas	0.94	0.93		
Uncultivated areas	0.86	0.88		
Dry areas	0.64	0.62		

RF Random Forest

Table 5 Disaster risk index (DRI) result for fluvial and pluvial floods with values obtained from the GEE platform of the Filyos River basin

Index				Grade and value				
Factor level		Indicator level		Very high	High	Medium	Low	Very Low
Factor	Weighted value	Indicator	Weighted value	(5)	(4)	(3)	(2)	(1)
F	W_F	I	W_I					
Hazard	0.45	Number of flood recurrences (year)	0.20	<2[a]	2–5	5–10	10–20	>20
		Size of the flood affected area (ha)	0.20	>50,000[a]	40,000–50,000	30,000–40,000	20,000–30,000	<20,000
		Standardized precipitation index (SPI)	0.20	>2.0	1.5–2.0[a]	1.0–1.5; 400–700[a]	0.0–1.0; 100–400	<0.0; <100
		Loss of forest areas (ha)	0.10	>1000	700–1000	300–400[a]	200–300	<200
		River flood index (m^3/s)	0.15	>500	400–500	10–15	5–10[a]	0–5
		Relative sea level rise in river delta (cm)	0.15	20–25	15–20	10–15	5–10[a]	<5
		–	[ ] = 1.0	–	–	–	–	–
Vulnerability	0.40	Population (person)	0.16	>600,000	450,000–600,000	300,000–450,000	150,000–300,000	<150,000
		SVI	0.10	–2.5–(–1.6)	–1.0–(–1.6)[a]	–0.5–(–1.0)	–0.2–(–0.5)	0.0–(–0.2)
		EVI	0.10	<0.00	0.01–0.20	0.20–0.25	0.25–0.4[a]	>0.4
		LST (°C)	0.10	>40	30–40	20–30[a]	10–20	<10
		Temperature (°C)	0.10	>40	30–40	20–30[a]	10–20	<10
		AOD	0.10	>30	20–30[a]	10–20	5–10	<5
		AET	0.10	>3	2.5–3.0[a]	2.0–2.5	1.5–2.0	<1.5
		Number of forest fires	0.12	>100	80–100[a]	60–80	40–60	<40
		Building density in delta and riverside (%)	0.12	>70[a]	55–70	40–55	25–40	<100
		–	[ ] = 1.0	–	–	–	–	–
Capability of preventing and reducing disaster	0.15	Observation frequency (months)	0.50	>24	12–24	6–12	3–6	<3[a]
		Urbanization level (%)	0.50	>70	55–70[a]	40–55	25–40	<25
	[ ] = 1.0	–	[ ] = 1.0	–	–	–	–	–

Disaster risk value for Filyos River basin

$F_1 = (I_{H1} \times W_{H1} + I_{H2} \times W_{H2} + I_{H3} \times W_{H3} + I_{H4} \times W_{H4} + I_{H5} \times W_{H5} + I_{H6} \times W_{H6}) = \mathbf{4}$

$F_2 = (I_{V1} \times W_{V1} + I_{V2} \times W_{V2} + I_{V3} \times W_{V3} + I_{V4} \times W_{V4} + I_{V5} \times W_{V5} + I_{V6} \times W_{V6} + I_{V7} \times W_{V7} + I_{V8} \times W_{V8} + I_{V9} \times W_{V9}) = \mathbf{4}$

$F_3 = (I_{A1} \times W_{IA1} + I_{A2} \times W_{IA2}) = \mathbf{3}$

$\mathbf{DRI = F_1 \times W_{F1} + F_2 \times W_{F2} + F_3 \times W_{F3}} = 4 \times 0.45 + 4 \times 0.40 + 3 \times 0.15 = \mathbf{4}$

[a]This is the severity class range for values obtained for the case study from the GEE platform

were examined using satellite images of different resolutions, and some were examined with data obtained from the databases on the platform. In order to evaluate the different characteristics of the indicators (especially resolution differences) together in the DRI analysis, the data were statistically averaged monthly, annually, and over long periods. The score that the statistical average values would receive from the disaster severity class was determined. The DRI index value, determined by the sum of the scores obtained from the disaster severity class multiplied by the weights, is four, and is considered as a categorically unacceptable risk. Based on the evaluations and the DRI method, it is apparent that the basin will face a significant risk of high hazards in the near future.

5 Conclusion

It has been shown that by using remote sensing and GIS together on the GEE platform for the application under consideration, different indicators and especially physical ecological indicators required for disaster risk assessment can be easily obtained. Determining these indicators using traditional methods is quite difficult and costly. It has been determined that thanks to this platform, which is open to development, large data storage is prevented, a large number of data and satellite images are obtained quickly, and different analyses can be performed on them. It has been determined that expanding the use of this platform will contribute to many areas and will also provide significant contributions to users in terms of time and cost.

It is known that the information obtained from the analyses made through the GEE platform is of great importance for land management (Long et al. 2019; Zeng et al. 2019; Amani et al. 2020; Du et al. 2021; Shastry et al. 2023; Abubakar et al. 2023; Waleed and Sajjad 2023). It has been observed that important information can be obtained with the findings obtained from the platform for this study, especially in terms of forest losses, control and supervision of forest fires, and sustainable forest structure. Additionally, the findings are vital for developing basin models, like flood and flood losses and productivity in agricultural lands. It is recommended that both urban and rural areas should adopt advanced technologies like GEE and remain receptive to innovations as part of sustainable land management practices. This approach can be useful in developing a comprehensive disaster risk plan and system.

In this study, as stated in the studies of Buyuksalih et al. (2005), Seker et al. (2005), and Akyüz et al. (2014), meanders and disconnected meander features have been observed in the Filyos River Delta and its surroundings. These features can create fluvial and pluvial flood risks, which have potential to damage nearby highways, airport, seaport, railway, and areas with dense structures. Fluvial and pluvial flood hazards within the basin are evaluated to pose a danger to the wellbeing, health, assets, and livelihood of individuals residing in the districts of Devrek, Çaycuma, and Gökçebey located in the Zonguldak Province, as well as in the Karabük Province and its Yenice district, in the context of population density. The assessment results of DRI are quite compatible with the findings of Seker et al. (2005) and Akyüz et al. (2014) in their studies of the basin. In these two studies, the parts of the Filyos River passing through the settlements determined above were found to be dangerous and risky. In addition, the technical analysis results of fluvial and pluvial floods that occurred on two different dates and were investigated within the scope of DRI evaluations also confirm this. Hence, it is necessary to adopt disaster management strategies and risk mitigation measures for those inhabiting the aforementioned regions of the basin.

As part of the DRI analysis conducted for the Filyos River basin, steps must be taken to decrease the high DRI score recorded in regions with high population density. Such measures will effectively lower exposure to hazards, protect individuals and their assets, enhance land and environmental protection, and prevent adverse events. Additionally, it is essential to acquire comprehensive disaster response skills through training. Raising awareness about disasters and implementing training and preparedness exercises, alongside the development of forecasting and warning systems previously non-existent in the basin, would aid in reducing risks. However, to decrease the potential hazards, crucial measures like activating municipal services, updating zoning plans according to the disaster in question, reorganizing land usage, and constructing buildings in accordance with appropriate regulations are necessary.

Acknowledgements The authors are thankful to the GEE cloud platform for freely available Landsat 8 OLI Sentinel-1 and MODIS images and the other datasets.

Funding Information Open access funding provided by the Scientific and Technological Research Council of Türkiye (TÜBİTAK).

Availability of data and material Data analyzed during the current study are available from the corresponding authors upon reasonable request.

Conflict of interest H. Akcin and R.T. Kose declare that they have no competing interests.

References

(2007) Directive 2007/60/EC of the European Parliament and of the Council on the assessment and management of flood risks. OJ L 288, p. 27–34. https://eur-lex.europa.eu/legal-content/EN/TXT/?uri=CELEX:32007L0060

Abubakar GA, Wang K, Koko AF, Husseini MI, Shuka KAM, Deng J, Gan M (2023) Mapping maize cropland and land cover in semi-arid region in northern Nigeria using machine learning and Google earth engine. Remote Sens 15:2835. https://doi.org/10.3390/rs15112835

Akcin H (2021) A GIS-based building risk assessment for the subsidence due to undercity coal mining activities in Zonguldak, Turkey. Arab J Geosci 14:376. https://doi.org/10.1007/s12517-021-06702-6

Akyüz DE, Kaya S, Seker DZ, Kabdasli S (2014) Definition of flood risky areas with calculation of stream water velocity via using numerical model: case study of Filyos River, Turkey. Fresenius Environ B 23:3022–3028

Amani M, Ghorbanian A, Ahmadi SA, Kakooei M, Moghimi A, Mirmazloumi SM, Moghaddam SHA, Mahdavi S, Ghahremanloo M, Parsian S, Wu Q, Brisco B (2020) Google earth engine cloud computing platform for remote sensing big data applications: a comprehensive review. IEEE J Sel Top Appl Earth Obs Remote Sens 13:5326–5350

Anaya JA, Gutiérrez VH, Pacheco AM, Palomino S, Han N, Balzter H (2020) Drivers of forest loss in a megadiverse hotspot on the pacific coast of Colombia. Remote Sens 12:1235. https://doi.org/10.3390/rs12081235

Bathrellos GD, Karymbalis E, Skilodimou HD, Gaki-Papanastassiou K, Baltas EA (2016) Urban flood hazard assessment in the basin of Athens Metropolitan city, Greece. Environ Earth Sci 75(4):319. https://doi.org/10.1007/s12665-015-5157-1

Buyuksalih I, Akcin H, Sefercik UG, Karakis S, Marangoz A (2005) Batı Karadeniz Sahil Bölgesindeki Filyos Nehri ve Deltasındaki Değişimlerin Zamansal GIS ile İncelenmesi (in Turkish). EGE Coğrafi Bilgi Sistemleri Sempozyumu (EGE Symposium on GIS), İzmir

Chang CL, Chao YC (2012) Using the analytical hierarchy process to assess the environmental vulnerabilities of basins in Taiwan. Environ Monit Assess 184(5):2939–2945. https://doi.org/10.1007/s10661-011-2162-z

Dalezios NR, Tarquis AM, Eslamian S (2017) Chapter 5 droughts. In: Dalezios NR (ed) Environmental hazards methodologies for risk assessment and management. International Water Association Publishing, London, pp 177–210

Deck O, Verdel T, Salmon R (2009) Vulnerability assessment for mining subsidence hazard. Int J Risk Anal 29(10):1380–1394

Du J, Kimball JS, Sheffield J, Pan M, Fisher CK, Beck HE, Wood EF (2021) Satellite flood inundation assessment and forecast using SMAP and landsat. IEEE J Sel Top Appl Earth Obs Remote Sens 14:6707–6715. https://doi.org/10.1109/JSTARS.2021.3092340

Hernández ML, Carreño ML, Castillo L (2018) Methodologies and tools of risk management: Hurricane risk index (HRi). Int J Disaster Risk Reduct 31:926–937. https://doi.org/10.1016/j.ijdrr.2018.08.006

Hu B, Zhou J, Wang J, Chen Z, Wang D, Xu S (2009) Risk assessment of land subsidence at Tianjin coastal area in China. Environ Earth Sci 59:269–276. https://doi.org/10.1007/s12665-009-0024-6

IFRAC (2023) International federation of red cross and red crescent societies. https://www.ifrc.org/our-work/disasters-climate-and-crises/what-disaster

IRDR (2014) Integrated Research on Disaster Risk-IRDR, Peril classification and hazard glossary. IRDR DATA Publication No. 1, Integrated Research on Disaster Risk, Beijing

Islam MS, Swapan MSH, Haque SM (2013) Disaster risk index: How far should it take account of local attributes. Int J Disaster Risk Reduct 3:76–87

Kandilioti G, Makropoulos C (2012) Preliminary flood risk assessment: the case of Athens. Nat Hazards 61(2):441. https://doi.org/10.1007/s11069-011-9930-5

Karmakar S, Simonovic SP, Peck A, Black J (2010) An information systemfor risk-vulnerability assessment to flood. J Geogr Inf Syst 2(03):129–146

Küçükali S (2019) Statistical investigation of Filyos river physical water quality parameters. Anatol Environ Animal Sci 4(3):519–524. https://doi.org/10.35229/jaes.636576

Long T, Zhang Z, He G, Jiao W, Tang C, Wu B, Zhang X, Wang G, Yin R (2019) 30 m resolution global annual burned area mapping based on Landsat Images and Google Earth Engine. Remote Sens 11(5):489. https://doi.org/10.3390/rs11050489

Mckee TB, Doesken NJ, Kleist J (1993) The relationship of drought frequency and duration to time scales. 8th Conference on Applied Climatology, Anaheim, 17–22 January 1993, pp 179–184

Peduzzi P (2006) The disaster risk index: overview of a quantitative approach. Measuring vulnerability to natural hazards: towards disaster resilient societies. United Nations University Press, Tokyo, New York, Paris, pp 171–181

Peng SH (2018) Preparation of a flood-risk environmental index: case study of eight townships in Changhua County, Taiwan. Environ Monit Assess 190:174. https://doi.org/10.1007/s10661-018-6540-7

Product User Guide European Relative Sea Level Rise explorer (2022) Issued by the climate data factory and B-open official reference number service contract: 2021/C3S2_430a. https://datastore.copernicus-climate.eu/documents/ecde/27-ecde-app-relative-sea-level-rise-v1.0.pdf

Product User Guide European River Flood explorer (2022) Issued by the climate data factory and B-open, official reference number service contract: 2021/C3S2_430a. https://datastore.copernicus-climate.eu/documents/ecde/16-ecde-app-river-flood-1.0.pdf

Ramli MWA, Alias NE, Yusop Z, Taib SM (2019) Disaster risk index: a review of local scale concept and methodologies. IOP Publ IOP Conf Ser Earth Environ Sc 479(2020):12023. https://doi.org/10.1088/1755-1315/479/1/012023

Rodriguez-Galiano VF, Ghimire B, Rogan J, Chica-Olmo M, Rigol-Sanchez JP (2012) An assessment of the effectiveness of a random forest classifier for land-cover classification. ISPRS J Photogramm Remote Sens 67:93–104. https://doi.org/10.1016/j.isprsjprs.2011.11.002

SAMHSA (2023) Substance abuse mental health services administration. https://www.samhsa.gov/find-help/disaster-distress-helpline/disaster-types

Şarlak N (2014) Filyos river streamflow reconstruction from treering chronologies with nonparametric approaches. J Am Water Resour Assoc 50:1102–1110. https://doi.org/10.1111/jawr.12172

Schumann AH, Schumann A, Nijssen D (2011) Application of scenarios and multi-criteria decision making tools in flood polder planning. In: Flood risk assessment and management. Springer Netherlands, Dordrecht, pp 249–275

Seker DZ, Kaya S, Musaoglu N, Kabdasli MS, Yuasa A, Duran Z (2005) Investigation of meandering in Filyos River by means of satellite sensor data. Hydrol Process 19:1497–1508. https://doi.org/10.1002/hyp.5593

Shastry A, Carter E, Coltin B, Sleeter R, McMichael S, Eggleston J (2023) Mapping floods from remote sensing data and quantifying the effects of surface obstruction by clouds and vegetation. Remote Sens Environ 291:113556. https://doi.org/10.1016/j.rse.2023.113556

Sönmez AY, Kale S (2020) Climate change effects on annual streamflow of Filyos River (Turkey). J Water Clim Chang 11(2):420–433. https://doi.org/10.2166/wcc.2018.060

Stefanidis S, Stathis D (2013) Assessment of flood hazard based on natural and anthropogenic factors using analytic hierarchy process (AHP). Nat Hazards 68:569–585. https://doi.org/10.1007/s11069-013-0639-5

Takamatsu M, Abhas J (2023) No mountain high enough: assessing geohazard risks using satellite technology in South Asia. United Nations office for the coordination of humanitarian affairs-OCHA, report of World Bank. https://blogs.worldbank.org/endpovertyinsouthasia/no-mountain-high-enough-assessing-geohazard-risks-using-satellite-technology

Thouret JC, Taillandier M, Arapa E, Wavelet E (2024) Vulnerable settlements to debris flows in Arequipa, Peru: population characteristics, hazard knowledge, risk perception, and disaster risk management. Natural Hazards 120:901–955. https://doi.org/10.1007/s11069-023-06167-8

Teh D, Khan T (2021) Types, definition and classification of natural disasters and threat level. In: Handbook of disaster risk reduction for resilience. Springer, Berlin Heidelberg, pp 27–56 https://doi.org/10.1007/978-3-030-61278-8_2

TOD (2022) Turkish forestry 2022: deforestation and forest degradation in Turkey. Turkish Foresters Association Publication, Ankara. ISBN 9786056897764 ((in Turkish). Editor: Erdoğan Atmiş. https://www.ormancilardernegi.org/icerik.ASP?ID=72)

UNEP (2023) The United Nations Environment Program Topics, Disasters and Conflicts. Available via DIALOG. https://www.unep.org/topics/disasters-and-conflicts

Van Westen CJ, Castellanos E, Kuriakose SL (2008) Spatial data for landslide susceptibility, hazard, and vulnerability assessment: an overview. Eng Geol 102(3):112–131. https://doi.org/10.1016/j.enggeo.2008.03.010

Waleed M, Sajjad M (2023) On the emergence of geospatial cloud-based platforms for disaster risk management: A global scientometric review of google earth engine applications. Int J Disaster Risk Reduct 97:104056. https://doi.org/10.1016/j.ijdrr.2023.104056

Wang Z, Lai C, Chen X, Yang B, Zhao S, Bai X (2015) Flood hazard risk assessment model based on random forest. J Hydrol 527:1130–1141. https://doi.org/10.1016/j.jhydrol.2015.06.008

Zeng H, Wu B, Zhang N, Tian F, Phiri E, Musakwa W, Zhang M, Zhu L, Mashonjowa E (2019) Spatiotemporal analysis of precipitation in the sparsely gauged Zambezi river basin using remote sensing and Google Earth Engine. Remote Sens 11(24):2977. https://doi.org/10.3390/rs11242977